ROYAL SOCIETY OF CHEMISTRY

PAPER

Check for updates

Mechanochemical synthesis of amorphous and crystalline Na₂P₂S₆ – elucidation of local structural changes by X-ray total scattering and NMR†

Charlotte Fritsch, Anna-Lena Hansen, [iD] * Sylvio Indris, [iD] Michael Knapp [iD] and Helmut Ehrenberg

The development of all-solid-state sodium-ion batteries as an alternative energy storage system to lithium based techniques demands for sodium conducting solid electrolytes and an understanding of the sodium conduction mechanism governed by the local structure of these glass-ceramic materials. Na₂P₂S₆ was synthesized in an amorphous state with subsequent crystallization. The change of the local structure before and after crystallization was analyzed in detail regarding the presence of structural building blocks such as $[P_2S_6]^{2-}$, $[P_2S_6]^{4-}$, $[P_2S_7]^{4-}$, and $[PS_4]^{3-}$. The structure of the crystalline phase differs markedly compared to the corresponding amorphous phase.

Introduction

All-solid-state post-lithium techniques demand for reliable, safe, and highly conducting sodium-based electrolytes. A promising class of solid electrolytes are thiophosphates and it was recently demonstrated that they can operate in full battery cells as electrolytes[1] or electrodes.[2,3] A use as electrocatalyst for water splitting is also intensely studied.[4,5] Despite these promising results, the reproducibility for the synthesis of amorphous materials remains challenging. One reason is the lack of understanding of structural peculiarities of these glasses. Therefore, detailed investigations of these materials are necessary. Without a full-scale understanding of the structural aspects the impact on ionic conductivity remains speculative.[6] As a result, significant differences in the microstructure and conductivity of solid state electrolytes are observed.[7–9]

Nevertheless, the use of amorphous materials could be seen as a future trend in further enhancing battery performance. Amorphous thiophosphates, compared to their crystalline analogues, are supposed to offer a better bulk conductivity because of a larger free volume for the conducting species and lower interfacial resistance.[6,10] It has recently been demonstrated that amorphous Li₃PS₄ shows a better performance than crystalline Li₃PS₄, that has been synthesized *via* subsequent crystallization of the amorphous Li₃PS₄.[9] Huang *et al.*

proposed a high amount of disorder to be crucial for the high mobility of Na-ions in amorphous Na₂Si₂O₅.[11] However, in crystalline Li₁₀GeP₂S₁₂ Li conductivity is higher compared to (Li₂S)(GeS₂)(P₂S₅) glass which can be attributed to a lower activation energy for diffusion along the Li-pathways in the crystal.[12] These contrary results emphasize the necessity for detailed investigations of solid state electrolytes.

The synthesis route of amorphous sodium thiophosphates through ball milling has been established by Hayashi *et al.*[8] for stoichiometries with high Na₂S contents of *x* = 0.67, 0.70, 0.75 and 0.80 in $x\text{Na}_2\text{S} + (1 - x)\text{P}_2\text{S}_5$. Surprisingly, no attempt was made to synthesize Na₂P₂S₆ in this study. Lotsch *et al.* described the synthesis of crystalline Na₂P₂S₆ starting from elements Na, P and S in vacuum-sealed silica glass tubes by heating at 1070 K for 10 h.[13] Different P–S building blocks that are known from crystalline and amorphous lithium and sodium containing thiophosphates with P in oxidation state 5+ are: *ortho*-$[PS_4]^{3-}$, *pyro*-$[P_2S_7]^{4-}$, and *meta*-$[P_2S_6]^{2-}$. Additionally, a *hypo*-$[P_2S_6]^{4-}$ unit exists with P in 4+ state. Unlike the corresponding crystalline material and the stoichiometry might suggest, a variety of these polyhedra can be present in the amorphous glasses. $[P_2S_6]^{4-}$ has been identified in a total scattering study of a lithium thiophosphate with a molar sulphide content of 75% instead of 50%, *i.e.* amorphous Li₃PS₄, which was also synthesized *via* ball milling.[9] Raman and ³¹P MAS NMR measurements indicated the presence of P–P linked $[P_2S_6]^{4-}$ in amorphous Li₇P₃S₁₁ and Li₄P₂S₇.[14] Zeier *et al.* found P–P linked "ethane-like" units surrounded by isolated $[PS_4]^{3-}$ tetrahedra in glassy Li₄P₂S₆ and isolated tetrahedra as glassy impurities in crystalline Li₄P₂S₆.[15] Less common ring or isobutane-like structures of P–S anions built from PS³⁻

Institute for Applied Materials – Energy Storage Systems (IAM-ESS), Karlsruhe Institute of Technology, Hermann-von Helmholtz-Platz 1, 76344 Eggenstein-Leopoldshafen, Germany. E-mail: anna-lena.hansen@kit.edu
†Electronic supplementary information (ESI) available: SEM images and detailed comparison of crystalline structures. See DOI: 10.1039/c9dt04777h

building blocks have been observed with Raman and NMR spectroscopy as reported by Zeier *et al.*[16] Furthermore, Ohara *et al.* were able to demonstrate with differential pair distribution function (d-PDF) analysis that during crystallization of Li_3PS_4 from $75:25$ $Li_2S:P_2S_5$ glass, the microstructure of the remaining glass phase did not change.[17]

In this paper, the structure of amorphous and crystalline $Na_2P_2S_6$ is investigated by means of X-ray diffraction (XRD), pair distribution function analysis (PDF), Raman spectroscopy and ^{23}Na and ^{31}P magic-angle spinning (MAS) nuclear magnetic resonance (NMR) spectroscopy.

Experimental

Based on the synthesis route described for Na_3PS_4, amorphous $Na_2P_2S_6$ was synthesized *via* mechanical milling of Na_2S and P_2S_5 according to eqn (1).[18,19]

$$Na_2S + P_2S_5 \rightarrow Na_2P_2S_6 \qquad (1)$$

A batch of 4 g of a stoichiometric mixture of Na_2S (Sigma Aldrich) and P_2S_5 (Honeywell-Fluka 99%) together with 70 g ZrO_2 balls with a diameter of 3 mm was ball milled in a ZrO_2 bowl of 45 mL using a planetary ball mill Pulverisette 7 Premium Line (Fritsch) under argon atmosphere at 510 rpm. Full amorphization of the starting materials was reached at 240 grinding cycles (5 min alternating with 15 min rest for cooling). Crystalline $Na_2P_2S_6$ is obtained through thermal annealing of amorphous $Na_2P_2S_6$. The amorphous material was calcined in Al_2O_3 crucibles sealed in quartz glass tubes under vacuum at 623 K for 10 h to reach crystallization. The heating and cooling rate was 2 K min^{-1}.

As a reference material for NMR and Raman spectroscopy, Na_3PS_4 was synthesized by the procedure described above using a molar concentration of 75% Na_2S and 25% P_2S_5. In contrast to $Na_2P_2S_6$, this phase already crystallizes during ball milling after only 30 min. Even after milling for 20 hours the sample remains crystalline.

Raman spectroscopy was performed on a LabRAM HR Evolution spectrometer (HORIBA Scientific) using a 100× magnification objective with an excitation wavelength of 632.81 nm. The spectral data were recorded with exposure times of 10 s over the wavenumber range of 100 to 1100 cm^{-1}. All samples were measured in sealed glass capillaries. All Raman spectra were baseline corrected using the Horiba Labspec 6 software.

X-ray diffraction patterns were collected after different milling times to determine the amorphization progress on a STOE Stadi P powder diffractometer using monochromatic Mo-K$_{\alpha1}$ radiation (λ = 0.70932 Å). Powder samples were measured in Debye Scherrer geometry in 0.5 mm diameter sealed glass capillaries.

The X-ray diffraction pattern of crystalline $Na_2P_2S_6$ was measured using a STOE Stadi P powder diffractometer with monochromatic Cu-K$_{\alpha1}$ radiation (λ = 1.54056 Å) in transmission geometry. The Rietveld Refinement of the diffraction

pattern was performed using the FullProf software package.[20] A Silicon reference (NIST640d) was utilized to account for instrumental contributions and alignment.

Room temperature synchrotron total scattering experiments were performed at the high-resolution powder diffraction beamline (P02.1) at PETRA III, DESY, using synchrotron radiation with a photon energy of 60 keV (λ = 0.20723 Å).[21] The diffraction patterns were acquired using a PerkinElmer area detector with a sample-detector distance of 350 mm. The exposure time for each diffraction pattern was 20 min. The obtained 2D images were integrated to 1D patterns by using the program DAWNscience.[22]

Powder samples were measured in sealed glass capillaries with 0.5 mm diameter. An empty capillary was measured under the same conditions and used for background subtraction. To account for the instrumental resolution function, LaB$_6$ (NIST660a) and a Ni reference were measured. The corresponding pair distribution function was calculated using pdfgetx3[23] with Q_{max} = 20 Å^{-1}. Calculation of PDFs based on molecular models and real space Rietveld fitting was performed with PDFgui.[24]

^{23}Na and ^{31}P MAS NMR spectra were obtained at a spinning speed of 20 kHz on a Bruker Avance 500 MHz spectrometer at a field of 11.7 T, which corresponds to resonance frequencies of 132.3 MHz (^{23}Na) and 202.5 MHz (^{31}P). For these measurements, the sample was packed into a 2.5 mm zirconia MAS rotor in an argon-filled glove box. The spectra were recorded with a rotor-synchronized Hahn-echo pulse sequence. We used 1 M NaCl to calibrate the chemical shift of ^{23}Na (0 ppm) and H_3PO_4 to calibrate ^{31}P (85%, 0 ppm).

Electrochemical impedance measurements were performed using a BioLogic SP300 potentiostat at frequencies from 1 MHz to 10 mHz with a 100 mV sinusoidal amplitude at 25 °C. A 8 mm pellet of 60 mg of the $Na_2P_2S_6$ material was sandwiched between stainless steel cylinders with a weight of 3 t. The sodium ion conductivity was calculated based on the equation:

$$\sigma = l/(A \cdot R) \qquad (2)$$

where σ is the ion conductivity, l is the pellet thickness, A is the pellet size and R is the resistance.

Scanning electron microscopy images were recorded using a Zeiss Merlin microscope using 10 kV acceleration voltage.

Results and discussion

Glass formation: chemical reaction through P–S bond breaking in P_2S_5

The time-dependent evolution of crystalline phases within the milled sample of Na_2S and P_2S_5 was determined by XRD as shown in Fig. 1. The reflections of the two starting materials Na_2S and P_2S_5 are initially superimposed after 0.5 h and 2 h of ball milling. After 20 h, the reflections disappeared completely. No additional reflections could be observed during the whole process of ball milling. In contrast to the sodium *ortho*-thio-
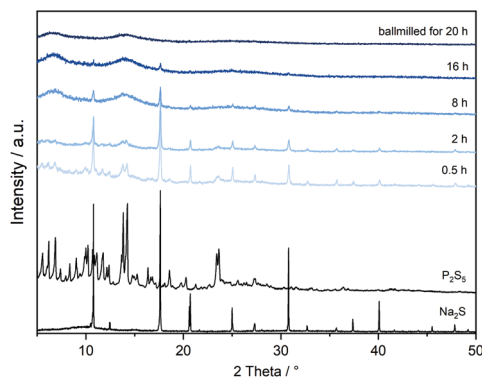
Fig. 1 Powder XRD patterns (Mo $K_{\alpha 1}$ radiation) of the binary starting materials Na_2S and P_2S_5, and of amorphous $Na_2P_2S_6$ after different milling times.

phosphate Na_3PS_4, $Na_2P_2S_6$ does not form a crystalline phase during ball milling.[25]

Based on Raman spectroscopy results the appearance of new modes depending on the milling time can be observed, indicating the formation of amorphous $Na_2P_2S_6$. After 1 h of milling, the Raman spectrum is still very similar to that of the starting substance P_2S_5 (Fig. 2). At this time, we also still observe large crystalline fractions of the starting materials Na_2S and P_2S_5 in the diffraction patterns (Fig. 1). After 8 h and 20 h ball milling time, signals from P–S vibrational modes occur in the Raman spectra which we attribute to the formation of $Na_2P_2S_6$.

In a previous work about glassy $Na_2P_2S_6$ synthesized by melt-quenching, the vibration mode 421 cm^{-1} was assigned to ν_{ring} P–S–P–S from $[P_2S_6]^{2-}$ and 578 cm^{-1} to ν_{as} PS$_3$ from the $[P_2S_6]^{4-}$ building block.[26]

Structure of crystalline $Na_2P_2S_6$

The structure of crystalline $Na_2P_2S_6$ was refined using the Rietveld method[27] based on the crystal structure published in 2014 by Lotsch et al.,[13] ISCD no. 426906. The corresponding X-ray diffraction pattern is shown in Fig. 3. $Na_2P_2S_6$ crystallizes in the monoclinic space group $P12_1/m1$ (no. 11). The lattice
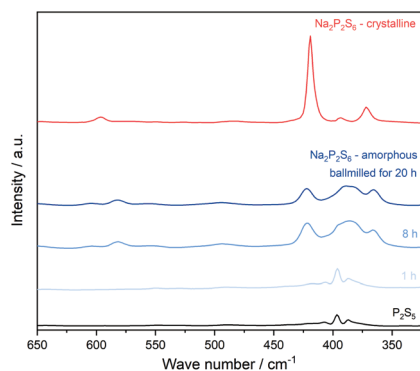

Fig. 2 Raman spectra of P_2S_5 and $Na_2P_2S_6$ after different milling times and after calcination (623 K for 6 h).

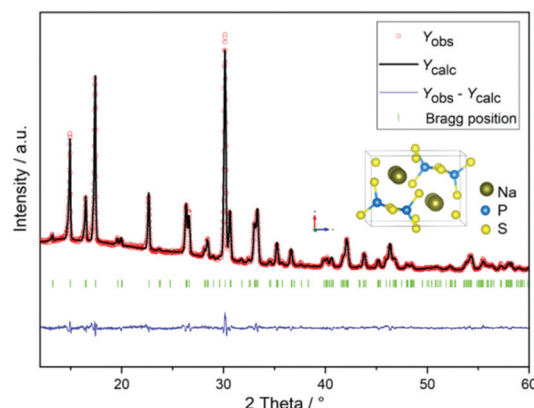**Fig. 3** Rietveld refinement of the powder diffraction pattern (Cu $K_{\alpha 1}$ radiation) of $Na_2P_2S_6$ and its crystal structure drawn with Vesta.[29]

parameters were refined to $a = 6.686(3)$ Å, $b = 7.831(4)$ Å, $c = 9.042(4)$ Å and $\beta = 90.22(4)°$. The results of Rietveld Refinement are given in Table 1 in the ESI.† The main building blocks of this crystal structure are *meta*-thiophosphate anions, *i.e.* two edge-sharing PS$_4$ tetrahedra (depicted in Fig. 3). No reflections from impurity phases could be detected. The PDF based on total scattering data collected at the high energy beamline P02.1 (DESY) could be fitted well up to at least 50 Å (Fig. 4).[28] Nevertheless, some peculiarities were encountered during the fitting process. The low r part of the PDF, especially the peak around 3.4 Å, could not be fitted well, when the fitted region exceeded ~20 Å, *i.e.* the intensity of the observed peak was higher than the one in the model. Most likely this is caused by a certain amount of local structural disorder, as often observed in structures built up by isolated polyhedral species. This peak belongs to S–S distances (detailed assignments are given in Fig. 6) of the edge-sharing tetrahedra.

This disorder could be covered by using anisotropic displacement factors, but only up to 20 Å. When the short range <5 Å is omitted in the fitting the resulting displacement factors become more isotropic, supporting the assumption

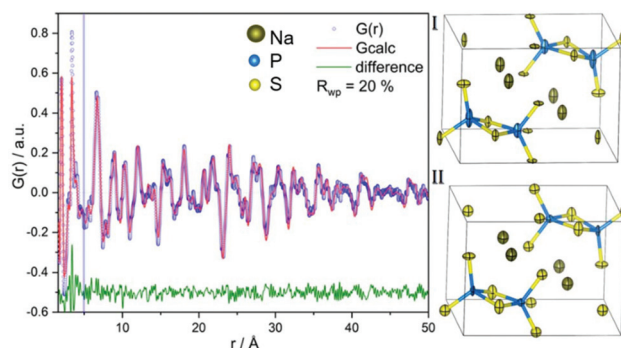**Fig. 4** Left: Real space Rietveld like least squares fitting of a calculated PDF based on $Na_2P_2S_6$ structural models given on the right. I: Result of fitting the whole range in real space 1.7–50 Å; II: Resulting structural model, when short range (*i.e.* 1.7–5 Å) is not included in the fit. Atoms are displayed by anisotropic displacement ellipsoids (probability of 50%).

that the disorder is a local phenomenon, which is averaged out on the global scale. Both models are compared in Fig. 4. The results of both refined structure models based on XRD and PDF, respectively, were compared using the program *Compstru* provided by the Bilbao Crystallographic Server.[30,31] The crystal structures coincide very well, indicated by a measure of similarity $\Delta = 0.016$, taking the lattice parameters and atomic coordinates into account.[32] The maximum deviation of atomic positions corresponding to the sodium ions yields a max. distance of 0.12 Å. Details can be found in the ESI.†

Amorphous *versus* crystalline structure

Since glasses are X-ray amorphous, meaning no reflections can be observed in an XRD pattern, synchrotron total scattering measurements were performed to calculate the corresponding pair distribution functions (PDF).[28] The normalized PDFs of the amorphous and crystalline sample are depicted in Fig. 5.

No intensity can be observed in the PDF of the amorphous sample above ~20 Å, indicating a fully random arrangement of the constituents. In the medium range ~5–18 Å the broad sinusoidal oscillation of the PDF, without distinct peaks, reveals that only a certain structural order, sometimes referred to as a kind of *pre ordering* of the main building units, but no strong correlations are present. The nature of these units can be discussed by having a closer look on the short-range order given in Fig. 6, which indicates both, agreements and disagreements with the local structure of the crystalline phase. The distances being present in *meta*-P_2S_6 are included as a reference. The most obvious difference is the absence of sodium related peaks in the PDF of the amorphous sample, marked by red lines in Fig. 6.

This indicates a high amount of sodium disorder within the glassy structure. Comparing the PDF of the amorphous sample with modelled PDFs of different thiophosphate anions, namely *ortho*-, *meta*-, *pyro*- and *hypo*-thiophosphate (Fig. S1†), reveals the difficulty to unambiguously determine the anionic species. However, due to the increased intensity of only the first peak at 2.1 Å, which can be assigned to P–S
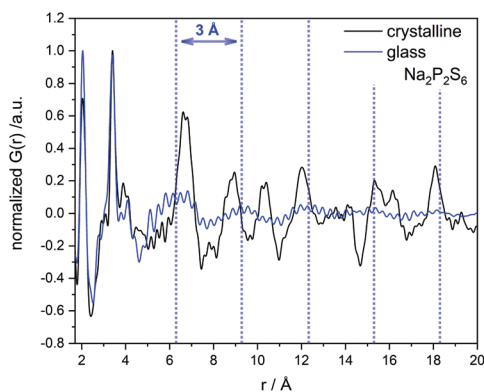

Fig. 6 Top: Comparison of short range of normalized PDF of amorphous (blue) and crystalline (black) $Na_2P_2S_6$. The corresponding distances based on literature reference $Na_2P_2S_6$ (ICSD_426906) are marked. Dotted grey lines correspond to distances occurring in *meta*-thiophosphate anion as depicted below. A represents P–S bond. Red lines correspond to sodium related distances, which are markedly less intense in the PDF of the amorphous material.

bonds, it can be assumed, that a higher amount of single $[PS_4]^{3-}$ tetrahedra is present in the sample. Furthermore, the presence of P–P linked $[P_2S_6]^{4-}$ can most likely be excluded. At 3.8 Å a pronounced signal is calculated for $[P_2S_6]^{4-}$ that can be assigned to the Gauche conformation of sulfur atoms along the P–P axis. This signal cannot be observed in the PDF. Therefore, we oppose the presence of this unit, in contrast to amorphous Li_3PS_4.[9]

With ^{23}Na and ^{31}P MAS NMR spectroscopy shown in Fig. 7, we can study the changes in the local environment around sodium and phosphorus atoms and compare them with known chemical shifts of similar structures, enabling a distinction between the differently linked P–S tetrahedra.

Fig. 5 Comparison of normalized PDF of amorphous (blue) and crystalline (black) $Na_2P_2S_6$. Dotted blue lines mark maxima of medium range modulations to emphasize the periodicity of 3 Å.
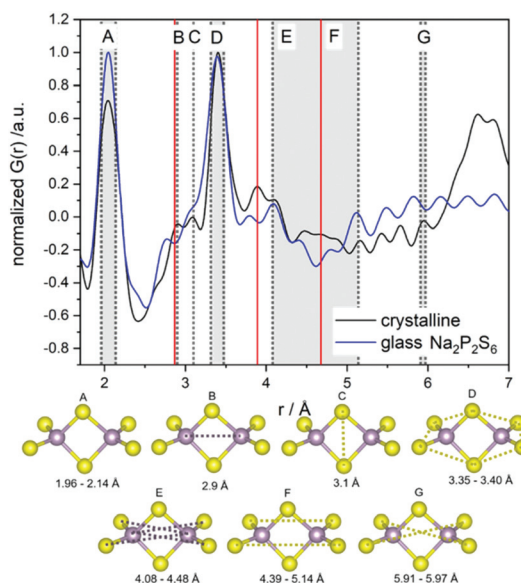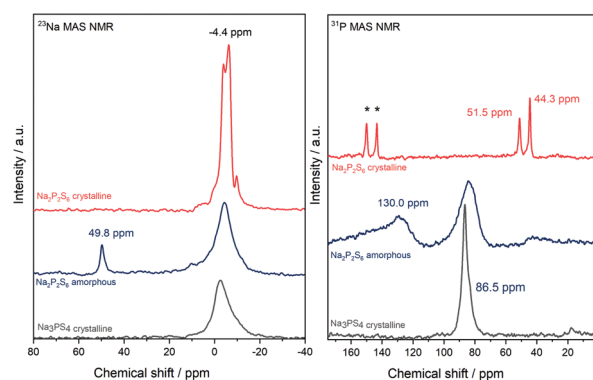

Fig. 7 ^{23}Na and ^{31}P MAS NMR spectra of amorphous and crystalline $Na_2P_2S_6$ and Na_3PS_4. Spinning sidebands are marked with an asterisk.

We can assign the signal at 86.5 ppm, being present in the ^{31}P MAS NMR spectra of crystalline Na_3PS_4, to isolated $[PS_4]^{3-}$ tetrahedra, in agreement with the well-known structure of Na_3PS_4.[14,33] This peak is very sharp for crystalline Na_3PS_4, revealing highly uniform $[PS_4]^{3-}$ tetrahedra in this highly crystalline structure. The two peaks observed for crystalline $Na_2P_2S_6$ at 44.3 and 51.5 ppm can be assigned to the two different phosphorus positions in this crystal structure belonging to two edge-sharing tetrahedra of the structural building block $[P_2S_6]$.[2] Both phosphorus atoms occupy a 2e position but are not crystallographically equivalent which we were able to determine from the crystal structure of the Rietveld refinement. The intensities of these two peaks are very similar when all spinning sidebands are used for integration. That is also in agreement with the structural information from Rietveld refinement: both P-atom positions are equally occupied.

The signal belonging to the isolated $[PS_4]^{3-}$ tetrahedra at 86.5 ppm is also observed for the amorphous $Na_2P_2S_6$ sample. We can therefore assume that this sample contains single tetrahedra and no corner-sharing tetrahedra like in the crystalline structure, since the chemical shifts of ^{31}P in the amorphous sample are different from those in the crystalline sample. The large width of this peak reflects strong variations in the bond angles and thus a distribution of resonance frequencies for this amorphous structure. The signal at 130.0 ppm of the amorphous sample can be assigned to corner-sharing tetrahedra.[14]

Sodium disorder

The ^{23}Na MAS NMR spectra reveal a signal at −4.4 ppm for all samples. The same position of the signal indicates that the chemical environment of sodium in the three thiophosphates is very similar, maybe also caused by the high mobility of Na in these materials. Again, the very narrow signal observed for crystalline $Na_2P_2S_6$, with clear indications of quadrupolar powder lineshapes (nuclear spin $I(^{23}Na) = 3/2$), reveals a well-defined local structure around Na in the well-crystalline sample while the broad peak observed for amorphous $Na_2P_2S_6$ is caused by local fluctuations in the environments around Na in the amorphous phase. We can assign the signal at 49.8 ppm in the amorphous $Na_2P_2S_6$ to a small amount of residual Na_2S educt.[34]

Ionic conductivity

From the Nyquist plot depicted in Fig. 8 we deduce an ionic conductivity of 5.7×10^{-8} S cm^{-1} for amorphous $Na_2P_2S_6$ and 2.6×10^{-11} S cm^{-1} for crystalline $Na_2P_2S_6$.

To the best of our knowledge, no ionic conductivity data is available in the literature on $Na_2P_2S_6$. Zeier et al. determined an ionic conductivity of 7.8×10^{-11} S cm^{-1} (ref. 35) for crystalline $Li_2P_2S_6$ at room temperature. The ionic conductivity of the amorphous $Na_2P_2S_6$ is significantly higher.

The improved ionic conductivity of $Na_2P_2S_6$ can therefore possibly be attributed to a higher degree of disorder of the Na ions, as indicated by PDF results.

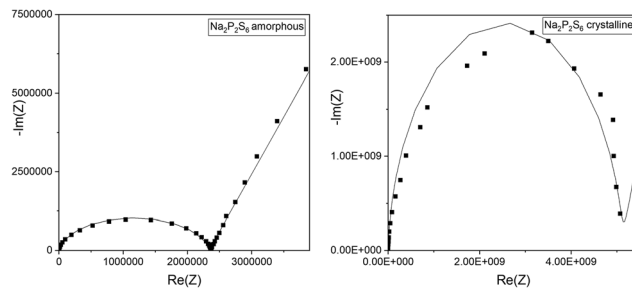**Fig. 8** Nyquist plot of electrical impedance measurement of amorphous and crystalline $Na_2P_2S_6$.

Conclusions

The long-range and local structures in amorphous and crystalline $Na_2P_2S_6$ and also their changes during synthesis have been observed by XRD, XRD-PDF analysis, Raman spectroscopy, and $^{23}Na/^{31}P$ MAS NMR spectroscopy. From the Raman spectrum we cannot distinguish between the different P–S subunits. The NMR spectrum of crystalline $Na_2P_2S_6$ shows two P signals that are in good agreement with the crystalline structure of $Na_2P_2S_6$ determined by Rietveld refinement. ^{31}P MAS NMR also shows a difference in the chemical shifts of crystalline and amorphous $Na_2P_2S_6$ revealing the presence of different local building blocks in these materials. Our measurements indicate that single PS_4^{3-} tetrahedra and corner-sharing tetrahedra are transformed to edge-sharing-tetrahedra during crystallization of amorphous $Na_2P_2S_6$ to crystalline $Na_2P_2S_6$.

Through this complementary use of material characterization techniques, the difference between an amorphous and crystalline structure of equal stoichiometry could be proven.

The difference in molecular structure with the same stoichiometry causes a difference in the material characteristics, which was demonstrated here by the ionic conductivity.

Conflicts of interest

The authors declare no competing interests.

Acknowledgements

diffraction measurement of P_2S_5 and Udo Geckle for the help with the SEM image recording.

Notes and references

1 N. Tanibata, M. Deguchi, A. Hayashi and M. Tatsumisago, *Chem. Mater.*, 2017, **29**, 5232.

2 C. Y. Fan, X. H. Zhang, Y. H. Shi, H. Y. Xu, J. P. Zhang and X. L. Wu, *J. Mater. Chem. A*, 2019, **7**, 1529.

3 B. H. Hou, Y. Y. Wang, Q. L. Ning, H. J. Liang, X. Yang, J. Wang, M. Liu, J. P. Zhang, X. Wang and X. L. Wu, *Adv. Electron. Mater.*, 2019, **5**, 1.

4 Q. Liang, L. Zhong, C. Du, Y. Luo, Y. Zheng, S. Li and Q. Yan, *Nano Energy*, 2018, **47**, 257.

5 C. F. Du, K. N. Dinh, Q. Liang, Y. Zheng, Y. Luo, J. Zhang and Q. Yan, *Adv. Energy Mater.*, 2018, **8**, 1.

6 T. Famprikis, P. Canepa, J. A. Dawson, M. S. Islam and C. Masquelier, *Nat. Mater.*, 2019, **18**, 1278.

7 S. S. Berbano, I. Seo, C. M. Bischoff, K. E. Schuller and S. W. Martin, *J. Non-Cryst. Solids*, 2012, **358**, 93.

8 K. Noi, A. Hayashi and M. Tatsumisago, *J. Power Sources*, 2014, **269**, 260.

9 H. Stöffler, T. Zinkevich, M. Yavuz, A. L. Hansen, M. Knapp, J. Bednarčík, S. Randau, F. H. Richter, J. Janek, H. Ehrenberg, *et al.*, *J. Phys. Chem. C*, 2019, **123**, 10280.

10 Q. Zhang, D. Cao, Y. Ma, A. Natan, P. Aurora and H. Zhu, *Adv. Mater.*, 2019, **31**, 1901131.

11 X. Lei, Y. Jee and K. Huang, *J. Mater. Chem. A*, 2015, **3**, 19920.

12 K. Mori, T. Kasai, K. Iwase, F. Fujisaki, Y. Onodera and T. Fukunaga, *Solid State Ionics*, 2017, **301**, 163.

13 A. Kuhn, R. Eger, J. Nuss and B. V. Lotsch, *Z. Anorg. Allg. Chem.*, 2014, **640**, 689.

14 C. Dietrich, D. A. Weber, S. J. Sedlmaier, S. Indris, S. P. Culver, D. Walter, J. Janek and W. G. Zeier, *J. Mater. Chem. A*, 2017, **5**, 18111.

15 C. Dietrich, M. Sadowski, S. Sicolo, D. A. Weber, S. J. Sedlmaier, K. S. Weldert, S. Indris, K. Albe, J. Janek and W. G. Zeier, *Chem. Mater.*, 2016, **28**, 8764.

16 M. Ghidiu, J. Ruhl, S. P. Culver and W. G. Zeier, *J. Mater. Chem. A*, 2019, **7**, 17735.

17 S. Shiotani, K. Ohara, H. Tsukasaki, S. Mori and R. Kanno, *Sci. Rep.*, 2017, **7**, 6972.

18 A. Hayashi, K. Noi, A. Sakuda and M. Tatsumisago, *Nat. Commun.*, 2012, **3**, 855.

19 T. Krauskopf, S. P. Culver and W. G. Zeier, *Inorg. Chem.*, 2018, **57**, 4739.

20 J. Rodríguez-Carvajal, *Phys. B*, 1993, **192**, 55.

21 A. C. Dippel, H. P. Liermann, J. T. Delitz, P. Walter, H. Schulte-Schrepping, O. H. Seeck and H. Franz, *J. Synchrotron Radiat.*, 2015, **22**, 675.

22 J. Filik, A. W. Ashton, P. C. Y. Chang, P. A. Chater, S. J. Day, M. Drakopoulos, M. W. Gerring, M. L. Hart, O. V. Magdysyuk, S. Michalik, *et al.*, *J. Appl. Crystallogr.*, 2017, **50**, 959.

23 P. Juhás, T. Davis, C. L. Farrow and S. J. L. Billinge, *J. Appl. Crystallogr.*, 2013, **46**, 560.

24 C. L. Farrow, P. Juhás, J. W. Liu, D. Bryndin, E. S. Božin, J. Bloch, Th. Proffen and S. J. L. Billinge, *J. Phys.: Condens. Matter*, 2007, **19**, 335219.

25 A. Hayashi, K. Noi, N. Tanibata, M. Nagao and M. Tatsumisago, *J. Power Sources*, 2014, **258**, 420.

26 C. Bischoff, K. Schuller, M. Haynes and S. W. Martin, *J. Non-Cryst. Solids*, 2012, **358**, 3216.

27 H. M. Rietveld, *J. Appl. Crystallogr.*, 1969, **2**, 65.

28 E. Takeshi and S. J. L. Billinge, in *Underneath the Bragg Peaks*, ed. T. Egami and S. J. L. Billinge, Pergamon, 2012, 55.

29 K. Momma and F. Izumi, *J. Appl. Crystallogr.*, 2011, **44**, 1272.

30 M. I. Aroyo, P.-M. J. Manuel, C. Cesar, K. Eli, I. Svetoslav, M. Gotzon, K. Asen and W. Hans, *Z Kristallogr. Cryst. Mater.*, 2006, **221**, 15.

31 G. de la Flor, D. Orobengoa, E. Tasci, J. M. Perez-Mato and M. I. Aroyo, *J. Appl. Crystallogr.*, 2016, **49**, 653.

32 G. Bergerhoff, M. Berndt, K. Brandenburg and T. Degen, *Acta Crystallogr., Sect. B: Struct. Crystallogr. Cryst. Chem.*, 1999, **55**, 147.

33 C. Bischoff, K. Schuller, N. Dunlap and S. W. Martin, *J. Phys. Chem. B*, 2014, **118**, 1943.

34 M. Krengel, A. L. Hansen, M. Kaus, S. Indris, N. Wolff, L. Kienle, D. Westfal and W. Bensch, *ACS Appl. Mater. Interfaces*, 2017, **9**, 21282.

35 C. Dietrich, D. A. Weber, S. Culver, A. Senyshyn, S. J. Sedlmaier, S. Indris, J. Janek and W. G. Zeier, *Inorg. Chem.*, 2017, **56**, 6681.